JOURNAL OF QUATERNARY SCIENCE (2018) **33**(1) 79–92 ISSN 0267-8179. DOI: 10.1002/jqs.3000

JQS Journal of Quaternary Science QRA Quaternary Research Association

Mid-Holocene Iberian hydroclimate variability and paleoenvironmental change: molecular and isotopic insights from Praia Rei Cortiço, Portugal

AUDREY K. TAYLOR,[1]* MICHAEL M. BENEDETTI,[1] JONATHAN A. HAWS[2] and CHAD S. LANE[1]
[1]Department of Earth and Ocean Sciences, University of North Carolina Wilmington, Wilmington, NC, USA
[2]Department of Anthropology, University of Louisville, Louisville, KY, USA

Received 21 October 2016; Revised 26 September 2017; Accepted 27 September 2017

ABSTRACT: At Praia Rei Cortiço (PRC), coastal Portugal, we analyzed compound-specific isotopes of plant wax-derived *n*-alkanes in combination with molecular distribution proxies and C/N ratios to reconstruct hydrologic and environmental change in a mid-Holocene wetland. During this relatively brief segment of the Holocene (6.6–5.4k cal a BP), substantial shifts in the stable hydrogen isotope composition of terrestrially sourced C_{29} *n*-alkanes ($\delta D_{n\text{-}C29}$) record significant multi-decadal changes in precipitation origin and storm trajectory. Wetland formation at PRC occurred during a humid interval (6.6–6.5k cal a BP) with a dominantly tropical precipitation source, likely the result of a persistent negative phase of the North Atlantic Oscillation, which permitted the establishment and dominance of *Sphagnum* moss. A subsequent decrease in precipitation significantly reduced *Sphagnum* abundance at PRC, which is evidenced by decreased sedimentary C/N ratios and reduced mid-chain *n*-alkane abundances. From 5.9 to 5.4k cal a BP, relatively low $\delta D_{n\text{-}C29}$ values coincide with sand invasion along the Iberian coast and cooling in the North Atlantic. Strong correspondence between $\delta D_{n\text{-}C29}$ values and the occurrence of ice-rafted debris recorded in deep sea sediment cores during this period illustrate a marked North Atlantic control on the trajectory of mid-latitude storms and precipitation regimes in Iberia. Copyright © 2017 John Wiley & Sons, Ltd.

KEYWORDS: ecotone; hydroclimate; Iberia; isotope; North Atlantic Oscillation.

Introduction

The Mediterranean is a climate-sensitive region that is especially vulnerable to future anthropogenic climate change (Giorgi, 2006). Regional temperature increases are expected to be greater than the global average and annual precipitation may be reduced by up to 40% (Giorgi and Lionello, 2008). The Mediterranean's susceptibility to such change is in part due to the supraregional influences of polar and tropical climatic perturbations (Trigo *et al.*, 2006), often demonstrated by the various atmospheric and oceanic oscillations that characterize the climatology of the Mediterranean basin. In the western Mediterranean, particularly the Iberian Peninsula, the North Atlantic Oscillation (NAO) is the dominant driver of regional climate variability (Lionello *et al.*, 2012). The NAO is associated with fluctuations in the intensity of the Icelandic Low and Azores High and consequent shifts in the position and strength of westerly flow (Hurrell *et al.*, 2001; Marshall *et al.*, 2001). Changes in the state of the NAO are commonly quantified using a positive or negative index, which is calculated based on the difference in winter sea level pressure between the two atmospheric masses. A more southerly mid-latitude storm track resulting from weakened high- and low-pressure systems occurs during negative phases of the NAO and increases winter storminess and precipitation over the Iberian Peninsula. Conversely, during positive phases of the NAO, storms instead track north through Europe and the Iberian Peninsula experiences dry and stable climatic conditions (Trigo *et al.*, 2002).

Annual and decadal modes of variability, such as the NAO, contribute to considerable uncertainties in projections of future European and Mediterranean hydroclimate (Visbeck *et al.*, 2001; Trigo *et al.*, 2006; Giorgi and Lionello, 2008). These uncertainties and the particular sensitivity of the Mediterranean region to changes in precipitation warrant investigations into the atmospheric response of the NAO to past large-scale climatic events and the resultant environmental impacts. Prehistoric records of the NAO have been derived using various proxies including stalagmite growth rates (Proctor *et al.*, 2000), sea salt concentrations in ice cores (Fischer and Mieding, 2005), speleothem oxygen isotopes (Smith *et al.*, 2016), and combined proxy–model methods (Trouet *et al.*, 2009). In Iberia, eolian records of dune migration and morphology are frequently used to determine NAO-induced changes in storm trajectory (Clarke and Rendell, 2006, 2009; Costas *et al.*, 2012, 2016). Characteristic of the NAO is a regional seesaw in which northern Europe and the Mediterranean exhibit asynchronous storminess and enhanced sand mobility, thus comparisons of lithological records of dune movement along the entirety of the European coast may be used to infer changes in atmospheric circulation related to the NAO (e.g. Clarke and Rendell, 2006, 2009; Costas *et al.*, 2012, 2016). Although these proxies provide substantial evidence of altered atmospheric processes, they often lack explicit evidence of the underlying mechanism of change, which is essential to improving predictions of future NAO behavior and other modes of climate variability (Trigo *et al.*, 2006).

One emerging method that has yet to be applied to Iberian hydroclimate reconstructions is the hydrogen isotopic measurement of isolated biomarkers, commonly referred to as compound-specific isotope analysis. Plant wax compounds, such as *n*-alkanes, have proven especially useful in paleoclimate applications of compound-specific isotope analysis (e.g. Tipple and Pagani, 2010; Tierney *et al.*, 2011;

*Correspondence: A. K. Taylor, as above.
E-mail: ataylo18@nd.edu

Schemmel *et al.*, 2016) as they are typically well preserved and abundant in sediments (Eglinton and Eglinton, 2008; Sachse *et al.*, 2012). Because *n*-alkanes are primarily composed of hydrogen from atmospheric source waters, they often retain the isotopic composition of paleoprecipitation (Sachse *et al.*, 2012), which records a geographic- and climate-dependent signature of precipitation amount, temperature, and source (Dansgaard, 1964). Despite an average apparent offset of approximately 125‰ between the stable hydrogen isotopic composition (δD) of plant wax and precipitation (Sachse *et al.*, 2004), which primarily results from evapotranspiration and lipid biosynthesis (Sachse *et al.*, 2012), hydrogen isotopic analyses of ancient *n*-alkanes allow for in-depth reconstructions of paleohydrology in a wide array of regional settings (e.g. Lane *et al.*, 2014; Moossen *et al.*, 2015; Schemmel *et al.*, 2016).

At a coastal site in central Portugal, Praia Rei Cortiço (PRC), the recent discovery of a mid-Holocene organic deposit presents the opportunity to employ compound-specific isotope analysis of terrestrial biomarkers as a proxy for paleohydrology and environmental change in an ecotonal region of the western Mediterranean. The δD of precipitation in Iberia is dominantly controlled by temperature and moisture source (Carreira *et al.*, 2005), and compound-specific hydrogen isotope analysis of *n*-alkanes in this region may be used to trace prehistoric changes in moisture transport, thus providing insight into the atmospheric mechanisms of hydrological change. Combined with compound-specific carbon isotope data, C/N ratios, and molecular distribution data, we document mid-Holocene Iberian hydroclimate variability and vegetation change in relation to the NAO and North Atlantic cooling.

Study area

Site description

PRC is located at 39.4°N on the Estremadura coast of central Portugal, approximately 75 km north of Lisbon near the mouth of the Óbidos lagoon (Fig. 1). Ecologically, the region is part of the Portuguese Coastal Superdistrict, characterized by limestone sea-cliffs and modern vegetation composed of juniper and oak with expansive communities of flowering shrubs and herbs (Costa *et al.*, 2000; Minckley *et al.*, 2015). Modern climate in this region is classified as sub-humid Mediterranean (Cfb); average annual temperature is ~16 °C and annual precipitation is approximately 670 mm, which is primarily received in winter.

Previous work at PRC has identified an abundance of paleoenvironmental information associated with eroding coastal bluffs, including an organic deposit (PRC-North; Fig. 1) dating to Marine Isotope Stage (MIS) 5d–5a (Minckley *et al.*, 2015), a Middle Paleolithic archaeological site (Haws *et al.*, 2010) and a Holocene paleosol capping 20 m of Pleistocene fluvial deposits (Benedetti *et al.*, 2009). These deposits occupy a buried paleovalley incised into Cretaceous conglomerate bedrock. A newly discovered section of organic sediment at the site (referred to here as PRC-South) outcrops in a younger incised

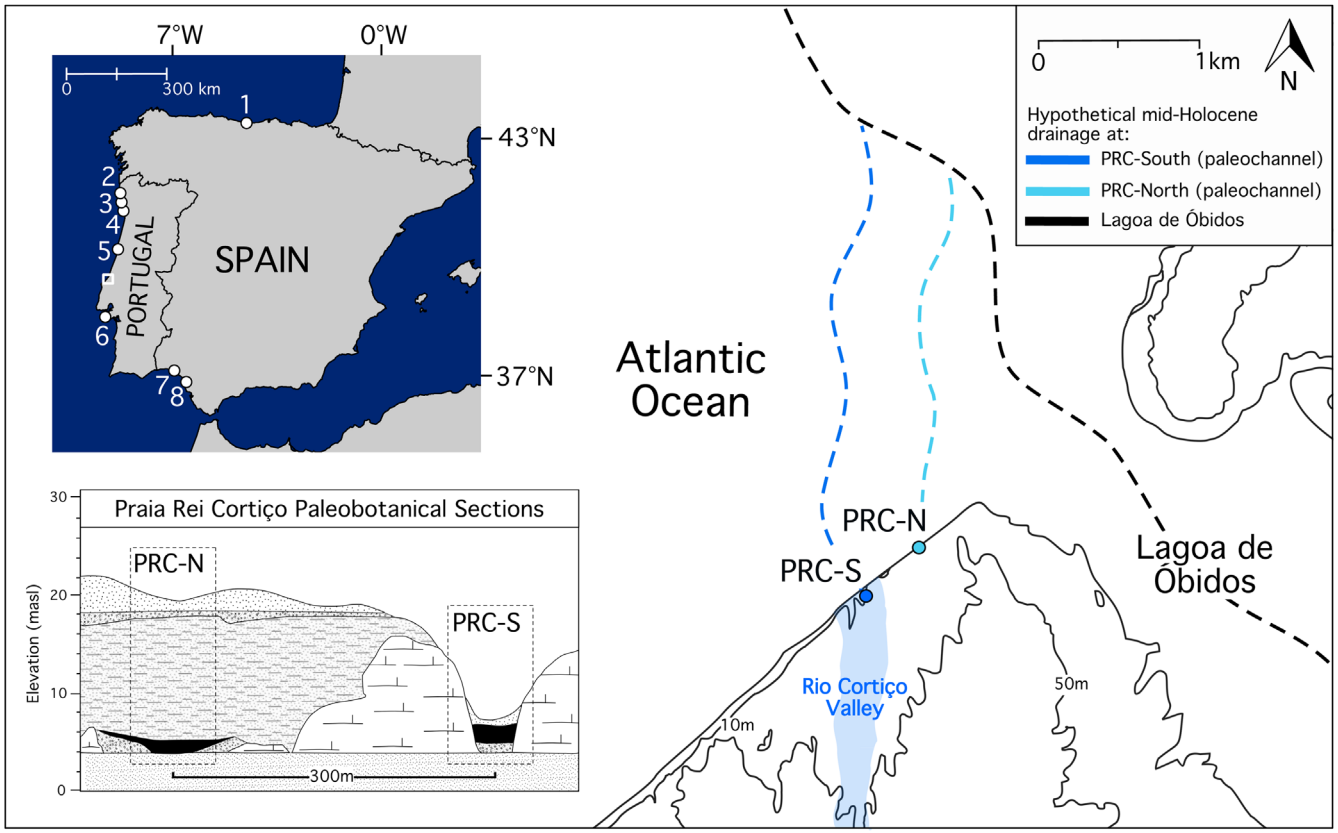

Figure 1. The positions and cross-sections of PRC-South, which is studied here, and PRC-North (Minckley *et al.*, 2015). The inferred mid-Holocene drainage of paleochannels at each site and the Lagoa de Óbidos are indicated by dashed lines. The inset map includes a regional overview and the locations of prior studies of Iberian mid-Holocene climate (1. Asturias, Ortiz *et al.*, 2010), sedimentary sequences representing Holocene paleowetlands in Portugal (2. Castelo do Neiva, Rebeiro *et al.*, 2011; 3. Esposende, Granja *et al.*, 2016; 4. Aguçadoura, Carvalho *et al.*, 2006; 5. Quiaios-Tocha region, Danielsen *et al.*, 2012), and coastal geomorphology (6. Caparica, Costas *et al.*, 2012; 7. Odiel estuary, Ruiz *et al.*, 2007; 8. Doñana National Park, Ruiz *et al.*, 2005).

valley at approximately the same elevation as PRC-North (4–6 m above mean sea level), but the two deposits are separated by roughly 300 m and a 20-m high bedrock divide (Fig. 1). PRC-South is a 2-m-thick organic fill that represents a mid-Holocene riparian wetland underlain by a pebbly sand fluvial channel deposit and overlain by several meters of eolian sand that have been partly disturbed by human activity at the surface (Fig. 2). The lower pebbly sand indicates that the Rio Cortiço was a freely meandering stream occupying an incised floodplain before wetland formation, which was likely related to the Holocene marine transgression. Holocene sea level rise along the Iberian coast was spatially variable, but in general, rapid sea level rise occurred until approximately 7 ka and was followed by a slow, more continuous rate of change until contemporary sea level was reached (Boski *et al.*, 2002; Costas *et al.*, 2016). In the lower Tagus valley, just 80 km south of PRC near Lisbon, sea level rise ceased at approximately 7 ka (Vis *et al.*, 2008) and is likely comparable to the timing at PRC. The region is tectonically active, but neotectonic movement along the central Portuguese coast has been negligible (Vis *et al.*, 2008). We propose that PRC was probably a former freshwater tributary of the Óbidos Lagoon, which currently empties into the Atlantic <1 km north (Fig. 1), and coastal barrier formation related to the deceleration of sea level rise after ~7 ka may have blocked the drainage of the valley, resulting in rising water tables and open water conditions with peat accumulation at PRC-South. Previous studies have demonstrated that a series of lagoons were established by sea level rise along the Iberian coast between 8.0 and 5.5 ka (Freitas *et al.*, 2002; Bao *et al.*, 2007; González-Villanueva et al., 2015), consistent with the timing of the inferred initial open water phase at PRC-South. Additionally, several sedimentary sequences in Portugal represent mid- to late Holocene paleolagoons or wetlands similar to PRC-South (Fig. 1), including interdune wetland deposits in the Quiaios-Tocha region (Danielsen *et al.*, 2012), an organic-rich mudstone at Castelo do Neiva beach (Rebeiro *et al.*, 2011), an organic deposit north of Esposende (Granja *et al.*, 2016), and a fine sedimentary unit containing peat and wood in the Aguçadoura Formation (de Carvalho *et al.*, 2006). PRC-South was sampled in 2013 and is the focus of the paleoenvironmental reconstruction presented here.

Isotopic composition of precipitation in Iberia

The isotopic composition of precipitation over the Iberian Peninsula primarily reflects the origin of air masses, temperature, and the mechanism of rainout (Carreira *et al.*, 2005). Modern mean annual precipitation at PRC averages about 600 mm and has an estimated annual δD value of −28‰, although average precipitation δD values fluctuate monthly by as much as 16‰ (Bowen and Revenaugh, 2003; IAEA/WMO, 2015; Bowen, 2017). Differences between monthly average δD values of modern precipitation in Iberia are likely representative of seasonal temperature variations, with summer rainfall being the most D-enriched and winter rainfall the most D-depleted (Araquás-Araguás and Diaz Teijeiro, 2005; Carreira *et al.*, 2005). However, when individual precipitation events are analyzed, moisture source and air mass trajectory largely influence δD values (Araquás-Araguás and Diaz Teijeiro, 2005; Carreira *et al.*, 2005). Due to Iberia's mid-latitudinal and southwestern location in Europe, the major sources of precipitation are tropical and North Atlantic water vapor transported by westerly circulation (Araguás-Araguás and

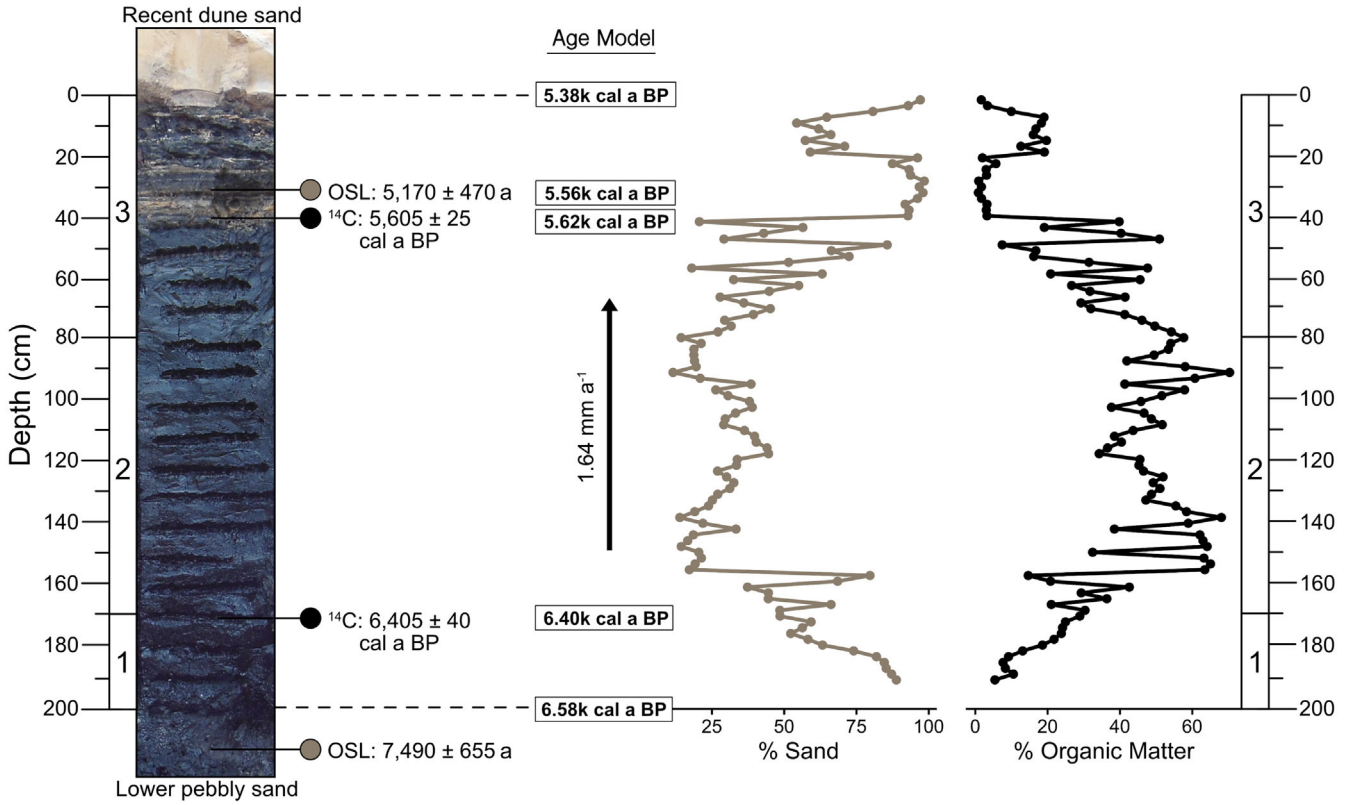

Figure 2. Summary of PRC-South stratigraphy, chronology and zonation (zones 1, 2, and 3). The age model presented was created using CLAM (Blaauw, 2010) and based on our two radiocarbon dates.

Diaz Teijeiro, 2005), which are two isotopically distinct moisture sources. In Paamiut, Greenland (62°N, 50°W), for example, the estimated annual δD value of precipitation is more negative than that of Miami, Florida (26°N, 80°W) by approximately 85‰ (Bowen and Revenaugh, 2003; IAEA/WMO, 2015; Bowen, 2017). Correspondingly, the most negative δD values of Iberian precipitation result from rainfall events associated with the advection of cold air masses from northern Europe and low-pressure centers located over Ireland, the British Islands, and the western North Atlantic (Araquás-Araguás and Diaz Teijeiro, 2005; Carreira *et al.*, 2005). Recycled moisture along the margin of the peninsula is negligible as a precipitation source during the wet season, but is significant during summer (Gimeno *et al.*, 2010). However, because summer is the dry season, we do not consider locally derived precipitation to be a dominant contributor to temporally integrated δD values at PRC.

Methods

Sedimentology

For compound-specific analyses, we sampled the PRC-South organic deposit at 10-cm intervals for a total of 21 samples. For bulk sediment analyses, we sampled the exposure more frequently at 2-cm intervals. Bulk sample organic matter and carbonate content (% by weight) were determined by loss on ignition (Heiri *et al.*, 2001) in an Omegaflux LMF 3550 muffle furnace. Samples were dried and crushed, then burned for 2.5 h at 550 °C for organic matter and 4 h at 950 °C for carbonates. The burned samples were then passed through a #230 standard mesh (63 μm) sieve to determine sand/mud content. For bulk C/N analysis, untreated sediment samples were dried at 60 °C and homogenized into a fine powder using a mortar and pestle. Analyses to measure percentage C and N were conducted using a Costech 4010 elemental analyzer paired with a Thermo Delta V Plus continuous flow mass spectrometer.

Age control

Organic material was isolated in the laboratory at 40 cm (charcoal) and 171 cm (wood) below the top of the deposit, and submitted for accelerator mass spectrometry radiocarbon dating at Beta Analytic, Inc. The IntCal13 database (Reimer *et al.*, 2013) and a linear age model in CLAM (Blaauw, 2010) were used to calibrate dates and establish a chronology for the deposit. Additional age control is provided by optically stimulated luminescence (OSL) ages on samples collected from the sandy layers interbedded within (30 cm) and underlying (215 cm) the PRC-South organic deposit. Samples used for OSL age determinations were collected by driving opaque PVC tubes into the face of the excavated outcrop, removing the sample, and capping the ends of the sample tube. The OSL ages were determined at the Luminescence Dating Research Laboratory, University of Illinois-Chicago, according to the modified multiple-aliquot regeneration procedure (Jain *et al.*, 2003). The specific laboratory techniques applied to OSL samples reported in this study are described by Minckley *et al.* (2015).

Compound-specific δD and $\delta^{13}C$ analyses

Long hydrocarbon chains, *n*-alkanes, are typically used for compound-specific hydrogen isotope analyses, in part because the environmental and biological modifications of precipitation δD are well studied and understood in these molecules. Before plant uptake, the preferential evaporation of lighter hydrogen contributes to D-enrichment of source water, and leads to the synthesis of hydrogen that is D-enriched relative to precipitation (Sachse *et al.*, 2012). The δD of plant wax lipids synthesized from leaf water is additionally influenced by transpiration, which has a similar enrichment effect (Sachse *et al.*, 2012). Despite these processes of D-enrichment, complex hydrogen exchange that occurs during *n*-alkane biosynthesis results in an average apparent fractionation of roughly −125‰ between precipitation δD and terrestrial lipid δD (Sachse *et al.*, 2012). Regardless of these fractionations, there are strong correlations between meteoric and biomarker δD (Sachse *et al.*, 2004), and sources of hydrogen fractionation in *n*-alkanes can be accounted for in analyses.

A discernible carbon isotopic distinction between C_3 and C_4 plants permits the use of compound-specific $\delta^{13}C$ for environmental reconstructions. Similar to compound-specific δD, compound-specific $\delta^{13}C$ measurements better constrain the isotopic signature of atmospheric CO_2, photosynthetic pathway, and climate that is recorded in plant tissues (Eglinton and Eglinton, 2008). Compared to other biochemical fractions (proteins, carbohydrates, lignin, etc.), lipids are the most depleted in ^{13}C (Galimov, 1985) and terrestrial *n*-alkanes typically have $\delta^{13}C$ values that are significantly lighter than bulk $\delta^{13}C$ values. For example, C_3 plant-derived *n*-alkane $\delta^{13}C$ values generally range between −39 and −31‰, and C_4 plant-derived *n*-alkane $\delta^{13}C$ values range between −25 and −18‰ (Bi *et al.*, 2005).

To isolate *n*-alkanes, sediment samples were dried, ground and sealed in a 2: 1 mixture of dichloromethane (DCM) and methanol and placed in Teflon bottles on a shaker table overnight. The total lipid extract was subsequently saponified to remove fatty acids, and the neutral lipid fraction was isolated using solid phase extraction with silica gel as the stationary phase and DCM as the eluting solvent. The aliphatic extract was further purified through the removal of branched and cyclic compounds with urea adduction and used for compound-specific isotope and molecular distribution analyses (Lane *et al.*, 2014).

Compound-specific carbon and hydrogen isotope analyses of *n*-alkanes were performed on a continuous-flow Thermo Delta V Plus mass spectrometer interfaced with a Thermo Trace 1310 gas chromatograph via a Thermo Isolink II interface using an RTX-5 silica column (60 m, 0.25-mm i.d., 0.50-μm film thickness). Injection temperatures were 320 °C and samples were injected with a Thermo AI1310 autosampler in surged split-less mode using high-purity helium as the carrier gas. The oven temperature program for the gas chromatograph was 70 °C isothermal for 1 min, 20 °C min^{-1} to 180 °C, 5 °C min^{-1} to 320 °C, and 320 °C isothermal for 20 min. High-purity hydrogen gas and *n*-alkane mixtures with known hydrogen isotope compositions were used as standards. The Indiana University *n*-alkane mixture (B4) was injected following every fourth sample to monitor precision of the instrument. The standard deviations of the standard analyses over the course of this study were <0.35‰ and <5‰ for carbon and hydrogen, respectively. For hydrogen isotope analyses, ^{3}H factors were calculated daily using the Isodat software with pulses of increasing amounts of reference gas. All samples were analyzed in duplicate and raw data were corrected using the uncertainty calculator spreadsheet created by Polissar and D'Andrea (2014). Hydrogen

isotopic compositions are reported in standard δ-per mil notation relative to VSMOW:

$$\delta D = 1000\ [(R_{sample}/R_{s\,tandard}) - 1]$$

where $R = {}^{2}H/{}^{1}H$. Carbon isotopic compositions are reported in standard δ-per mil notation relative to VPDB:

$$\delta^{13}C = 1000\ [(R_{sample}/R_{s\,tandard}) - 1]$$

where $R = {}^{13}C/{}^{12}C$.

Molecular distribution

Lipid abundance was determined using a Thermo Trace 1310 gas chromatograph via flame ionization detection. Compounds were separated on a 60-m RTX-5 column (0.25-mm i.d., 0.50-μm film thickness) in surged splitless mode with He as the carrier gas. Oven temperature was programmed from 70 °C (held for 1 min) to 180 °C at 20 °C min^{-1} and subsequently to 320 °C at 5 °C min^{-1} (held for 20 min). An external standard containing all *n*-alkanes from C_4 to C_{40} was used to identify and quantify *n*-alkane abundances.

n-Alkane indices

Differences in predominant *n*-alkane production between aquatic and terrestrial plant communities allow for broad classifications of vegetation types based on the molecular distribution of carbon chain lengths. Terrestrial plant wax is primarily composed of long chain *n*-alkanes (C_{25}–C_{35}) with a strong odd over even predominance (Sachse *et al.*, 2012). A carbon preference index (CPI) is typically used to differentiate between terrestrial plant and diagenetic origins of *n*-alkanes and is calculated according to Marzi *et al.* (1993) as:

$$CPI = \left[\sum_{odd}(C_{21} - C_{31}) + \sum_{odd}(C_{23} - C_{33})\right] / \left[2\sum_{even}(C_{22} - C_{32})\right]$$

CPI values >1 indicate a primarily terrestrial plant source of *n*-alkanes, as odd carbon chain lengths are more abundant than even carbon chain lengths. Aquatic plants also produce dominantly odd-chain *n*-alkanes, but typically have shorter chain lengths (C_{21}–C_{25}). A proxy ratio of *n*-alkane abundances, P_{aq}, is frequently used to identify the input of submerged aquatic macrophytes relative to that of terrestrial plants and can be used to quantify changes in past plant communities (Ficken *et al.*, 2000). Similar to aquatic vegetation, *Sphagnum* mosses predominantly produce *n*-C_{23} and *n*-C_{25} (Baas *et al.*, 2000; Nott *et al.*, 2000; Pancost *et al.*, 2002), and fluctuations in *Sphagnum* cover are also recorded by P_{aq}. Due to the hydrologic control on *Sphagnum* extent, P_{aq} in peatlands may be used alternatively as a paleohydrologic indicator (Nichols *et al.*, 2006).

P_{aq} was calculated according to Ficken *et al.* (2000):

$$P_{aq} = (C_{23} + C_{25})/(C_{23} + C_{25} + C_{29} + C_{31})$$

To accentuate changes within the terrestrial vegetation community, we apply the Norm31 index (e.g. Carr *et al.*, 2014). Because Norm31 only takes the abundances of *n*-C_{29} and *n*-C_{31} into account, it may demonstrate temporal variability in long-chain *n*-alkane production related to terrestrial vegetation composition. Norm31 is calculated as:

$$Norm31 = \frac{C_{31}}{(C_{31} + C_{29})}$$

Results

Chronology

Radiocarbon dates indicate that the organic deposit at PRC-South encompasses a 1200-year period, spanning from approximately 6.6 to 5.4k cal a BP. This is based primarily on extrapolation from two radiocarbon ages (Fig. 2; Table 1) calibrated using the IntCal13 database (Reimer *et al.*, 2013). A linear age model processed in CLAM (Blaauw, 2010) estimates ages of 6583 ± 99 BP at the bottom and 5383 ± 61 BP for the top of the organic deposit (Fig. 2; Table S1), yielding a sedimentation rate of 1.64 ± 0.14 mm a^{-1} during this interval. These ages are roughly estimated and associated with considerable uncertainty, as our ability to precisely constrain chronology is limited by only two radiocarbon dates and extrapolation. However, the OSL samples provide additional confirmation of the age model (Table 2). The OSL age of 7490 ± 655 a from pebbly sands below the organic deposit pre-dates the maximum age of the organic deposit that was estimated according to radiocarbon dates. The OSL age of 5170 ± 490 a from a sandy lens near the top of the organic deposit (30 cm) overlaps with the radiocarbon age from 10 cm lower in the section (Table 1). These ages demonstrate that the PRC-South organic deposit is approximately the same age as the Holocene paleosol overlying the archeological and paleobotanical sections previously investigated at PRC (Haws *et al.*, 2010; Minckley *et al.*, 2015). Both the PRC paleosol and the PRC-South organic deposit are buried by late Holocene eolian sands that mantle much of the Estremadura coastline (Benedetti *et al.*, 2009).

Stratigraphy

The PRC-South organic deposit is primarily composed of sand and organic matter (Fig. 2), with low mud content (<35%) and minor amounts of carbonate (<4%). Sand ranges from 11.5 to 98.5% with notable interbedding of sandy and organic lenses at the top of the deposit. Organic matter content ranges from 0.85 to 70.3% and dominates the middle of the deposit. We divided the PRC-South deposit into three

Table 1. PRC-south radiocarbon age results.

Depth in section (cm)	Laboratory code	Material	$\delta^{13}C$ (‰)	Conventional ^{14}C age (a BP)	Intercept with calibration curve (cal a BP)	2σ Calibrated ^{14}C age range (cal a BP)*
40	Beta-423463	Charcoal	−26.0	4890 ± 30	5605	5655–5590
171	Beta-394095	Wood	−24.3	5630 ± 30	6405	6470–6390

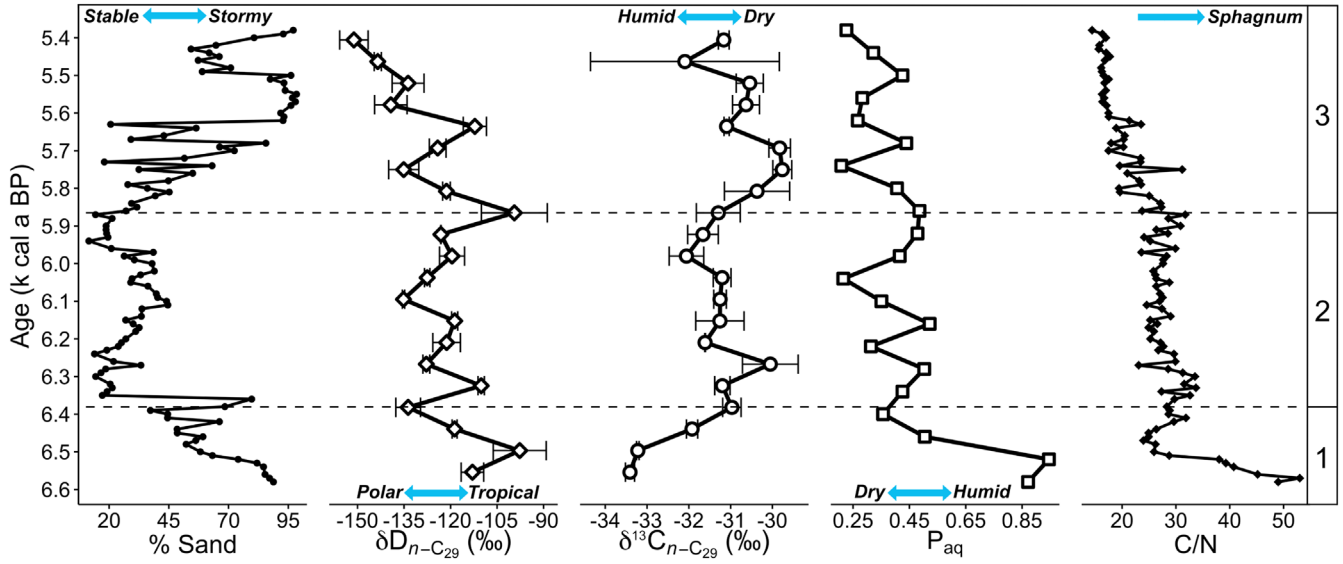

Figure 3. Summary and stratigraphic zonation (zones 1, 2, and 3 indicated on the right) of proxy data from PRC-South, including per cent sand, δD values of the C_{29} *n*-alkane ($\delta D_{n\text{-}C29}$), $\delta^{13}C$ values of the C_{29} *n*-alkane ($\delta^{13}C_{n\text{-}C29}$), per cent aquatic vegetation/*Sphagnum* moss expressed in decimal form (P_{aq}), and C/N values. Arrows represent our general interpretation of each proxy.

stratigraphic zones on the basis of the gross sedimentology of the deposit: Zone 1 (200–170 cm) contains coarse sands intermixed with organic matter, Zone 2 (170–80 cm) is a dark organic-rich section with low sand content, and Zone 3 (80−0 cm) is a layer of organic matter interbedded with medium to fine sand.

Compound-specific δD and compound-specific $\delta^{13}C$ values

The δD values of the C_{29} and C_{31} *n*-alkanes have ranges of 53.5‰ (−151.2 to −97.7‰) and 49.2‰ (−172.1 to −122.9‰), respectively. The δD values of *n*-C_{23}, *n*-C_{25} and *n*-C_{27} are more variable with ranges of 140.3‰ (−265 to −124.7‰), 89.4‰ (−199.2 to −109.8‰) and 66‰ (−182.2 to −116.2‰), respectively. Although overall trends between chain lengths are generally similar, absolute δD values of *n*-C_{23}, *n*-C_{25} and *n*-C_{27} are on average 33, 46 and 32‰ more depleted in D than *n*-C_{29}, respectively. Notable trend contrasts and substantial differences in δD between middle (defined here as C_{23}, C_{25} and C_{27}) and long chain lengths (C_{29} and C_{31}) occur in Zone 1 and at 5.7k cal a BP (Fig. S1). A comparable distinction between middle and long-chain *n*-alkanes is also evident in the compound-specific $\delta^{13}C$ values (Fig. S2), although absolute values are fairly similar and all homologues have ranges between 1.9 and 4.5‰. Compound-specific $\delta^{13}C$ values of *n*-C_{29} and *n*-C_{31} have ranges of 3.6 (−33.4 to −29.8‰) and 2.5 (−32.9 to −30.4‰), respectively. The $\delta^{13}C$ values of *n*-C_{23}, *n*-C_{25} and *n*-C_{27} have ranges of 2 (−32.7 to −30.7‰), 4 (−32.1 to −28.1‰) and 4.5 (−32.1 to −27.6‰), respectively.

Stratigraphic zonation

The stable hydrogen isotopic composition of *n*-C_{29} ($\delta D_{n\text{-}C29}$) in Zone 1 (6.6–6.4k cal a BP) has a range of 36‰ and becomes more negative towards the top of the zone. The stable carbon isotopic composition of *n*-C_{29} ($\delta^{13}C_{n\text{-}C29}$) trends towards more positive values, increasing by 2.3‰ (Fig. 3). From 6.6 to 6.5k cal a BP, mid-chain *n*-alkanes dominate molecular distributions, which is reflected by deposit maximum P_{aq} values. The highest C/N values in the deposit also occur during this time, with a maximum value of 53 at 198.5 cm (Fig. 3). After 6.5k cal a BP, there is a marked reduction in mid-chain *n*-alkanes which coincides with substantially decreased C/N ratios. P_{aq} decreases from 0.945 to 0.356 (Fig. 3) and Norm31 values vary minimally, ranging between 0.57 and 0.63 (Fig. S3). CPI values in this zone range from 6.26 to 16.03 and, although variable, indicate a primarily plant wax origin of *n*-alkanes (Table S1; Fig. S3).

In Zone 2 (6.4–5.9k cal a BP), $\delta D_{n\text{-}C29}$ values are variable with a range of ∼36‰, but transitions and absolute values are moderate relative to the rest of the deposit (Fig. 3).

Table 2. Optically simulated luminescence (OSL) ages and associated chronological data for sediments from PRC-South (12 November 2015).

Depth in section (cm)	Laboratory code	Equivalent dose (Gy)*	U (ppm)†	Th (ppm)†	K (%)†	Organic matter (%)	H_2O (%)	Cosmic dose (mGy a^{-1})‡	Total dose rate (mGy a^{-1})	OSL age (a)§
30	UIC3583	4.27 ± 0.31	1.1 ± 0.1	1.7 ± 0.1	0.48 ± 0.01	3 ± 0.5	15 ± 3	0.18 ± 0.02	0.83 ± 0.04	5170 ± 490
215	UIC3584	7.66 ± 0.51	1.2 ± 0.1	4.4 ± 0.1	0.43 ± 0.01	0	15 ± 3	0.14 ± 0.01	1.02 ± 0.05	7490 ± 655

*Equivalent dose was determined using the coarse-grained (475−525 μm) quartz fraction by the multiple aliquot regenerative dose method under blue (470 nm) excitation after infrared excitation (Jain *et al.*, 2003). Blue emissions are measured with 3-mm-thick Schott BG-39 filters and one, 3-mm-thick Corning 7-59 glass filter that blocks >90% luminescence emitted below 390 nm and above 490 nm in front of the photomultiplier tube.

†U, Th and K_2O determined by ICP-MS, Activation Laboratory, Ltd, Ontario.

‡Cosmic dose rate component from Prescott and Hutton (1994).

§All errors are at one sigma and ages represent years before AD 2010.

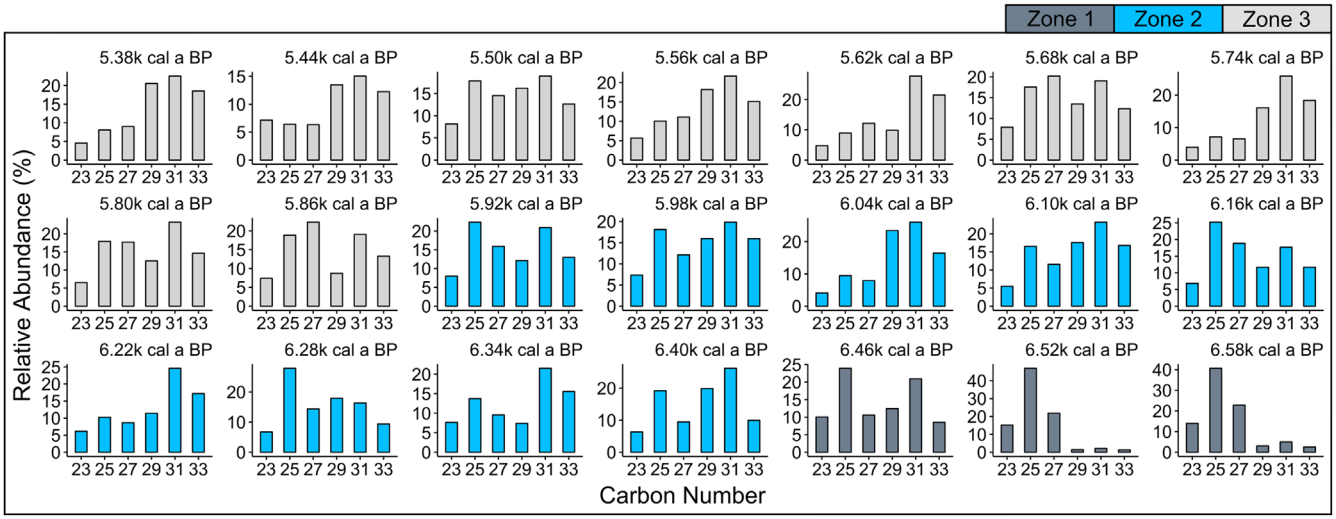

Figure 4. Per cent relative abundance of odd-numbered *n*-alkanes C_{23}–C_{33} in each stratigraphic zone at PRC-South between roughly 5.4 and 6.6k cal a BP.

Molecular proxies and bulk geochemical data show similar variation with minor changes compared to Zone 1. Norm31 values range from 0.48 to 0.75 (Fig. S3) and P_{aq} has a range of 0.307 (Fig. 3). C/N values remain stable around ~30 and $\delta^{13}C_{n\text{-}C29}$ values are also uniform throughout this zone, fluctuating by <2‰ (Table S1). A continued plant wax origin of *n*-alkanes is indicated by CPI values, which range between 6.26 and 16.77 and demonstrate an overall increase in Zone 2 (Fig. S3).

Zone 3 (5.9–5.4k cal a BP) is characterized by a progressive and significant transition towards more negative $\delta D_{n\text{-}C29}$ values. The hydrogen isotopic composition of C_{29} *n*-alkanes throughout this section has a range of 51.8‰ with −151.2‰ at 5.4k cal a BP as the most negative value in the entire deposit (Fig. 3). Compound-specific $\delta^{13}C_{n\text{-}C29}$ values are slightly more variable in this zone, but fluctuate by only 2.3‰. P_{aq} decreases from 0.486 to 0.226 and C/N values continue to decline, reaching a deposit minimum value of 14.4 at the top of the deposit (Fig. 3). C_{max}, the dominant carbon chain-length, is C_{31} throughout most of this section, with exceptions at 5.9 and 5.7k cal a BP where C_{27} is instead the most abundant homologue (Fig. 4). Norm31 values generally decrease throughout this zone and have a range of 0.23. CPI values are variable, fluctuating between 2.02 and 13.71 (Table S1; Fig. S3).

Discussion

Site geomorphology and vegetation composition

The initial predominance of C_{23} and C_{25} *n*-alkanes (Fig. 4), lower concentrations of longer chain lengths, and C/N ratios of ~50 (Fig. 3) at PRC-South indicate the presence of *Sphagnum*, a non-vascular moss (van Breemen, 1995; Baas *et al.*, 2000; Nott *et al.*, 2000; Pancost *et al.*, 2002). A mid-chain *n*-alkane molecular distribution of $C_{25} > C_{27} > C_{23}$ (Fig. 4) is likely indicative of a hummock *Sphagnum* species similar to *S. fuscum* of the section Acutifolia (Bingham *et al.*, 2010; Andersson *et al.*, 2011). In the Estremadura region, *Sphagnum* moss is currently rare (Seneca, 2003), and its prehistoric occupation at the PRC-South wetland represents a unique niche situated at the southern border of its modern-day ecological limits in Europe. *Sphagnum* mosses in Portugal typically inhabit the northwestern coastal zone and the high altitudes of the central mountain ranges (Seneca, 2003). Unlike most of the limestone coast of Estremadura, the PRC site is underlain by a siliciclastic conglomerate bedrock, which probably contributed to acidic and nutrient-poor soil conditions that favored the establishment of a localized *Sphagnum* population. The long-chain *n*-alkane predominance of C_{31} throughout most of the PRC-South deposit is probably representative of Ericaceous shrubs (Pancost *et al.*, 2002), which inhabit much of the Portuguese coast (Costa *et al.*, 2000) and are commonly abundant in *Sphagnum* wetlands.

The past occurrence of *Sphagnum* moss at PRC-South is representative of a freshwater wetland, probably a fen or bog. A pollen-based study by Minckley *et al.* (2015) determined that PRC-North was also a near-coast freshwater wetland between MIS 5d and 5a (roughly 110–80 ka) with vegetation at the site primarily consisting of wetland taxa such as Ericaceae, Poaceae and Cyperaceae surrounded by Mediterranean and temperate forest represented mainly by *Pinus* spp. and *Quercus* spp. (Minckley *et al.*, 2015). The coastal ecosystems at PRC during the previous and current interglacial may have been similar to those of modern-day Doñana National Park in southwestern Spain, which is composed of a series of transgressive coastal dunes, back-barrier lagoons, and peat bogs dominated by heath vegetation, scrubland, and pine and cork oak forests (Corona *et al.*, 1988; Muñoz-Reinoso, 2001; Sousa *et al.*, 2013). In particular, the Doñana peat bogs known as 'Rivatehilos' are characterized by the presence of *Erica ciliaris* wet heathland and other vegetation, including various *Sphagnum* mosses, which are more typically found in the north-western Iberian margin (Sousa *et al.*, 2013).

Environmental δD_{wax} controls at PRC-South

The hydrogen isotopic composition of sedimentary *n*-alkanes integrates a combination of various climatic and environmental parameters, which can make it difficult to discern the primary source of δD variability over time. Despite a general −125‰ apparent fractionation between precipitation and plant wax δD (Sachse *et al.*, 2004), the δD of individual plant species within the same catchment area can vary significantly. For example, Hou *et al.* (2007) observed differences in δD of as much as 70‰ between terrestrial vegetation types (trees, ferns, grasses) surrounding

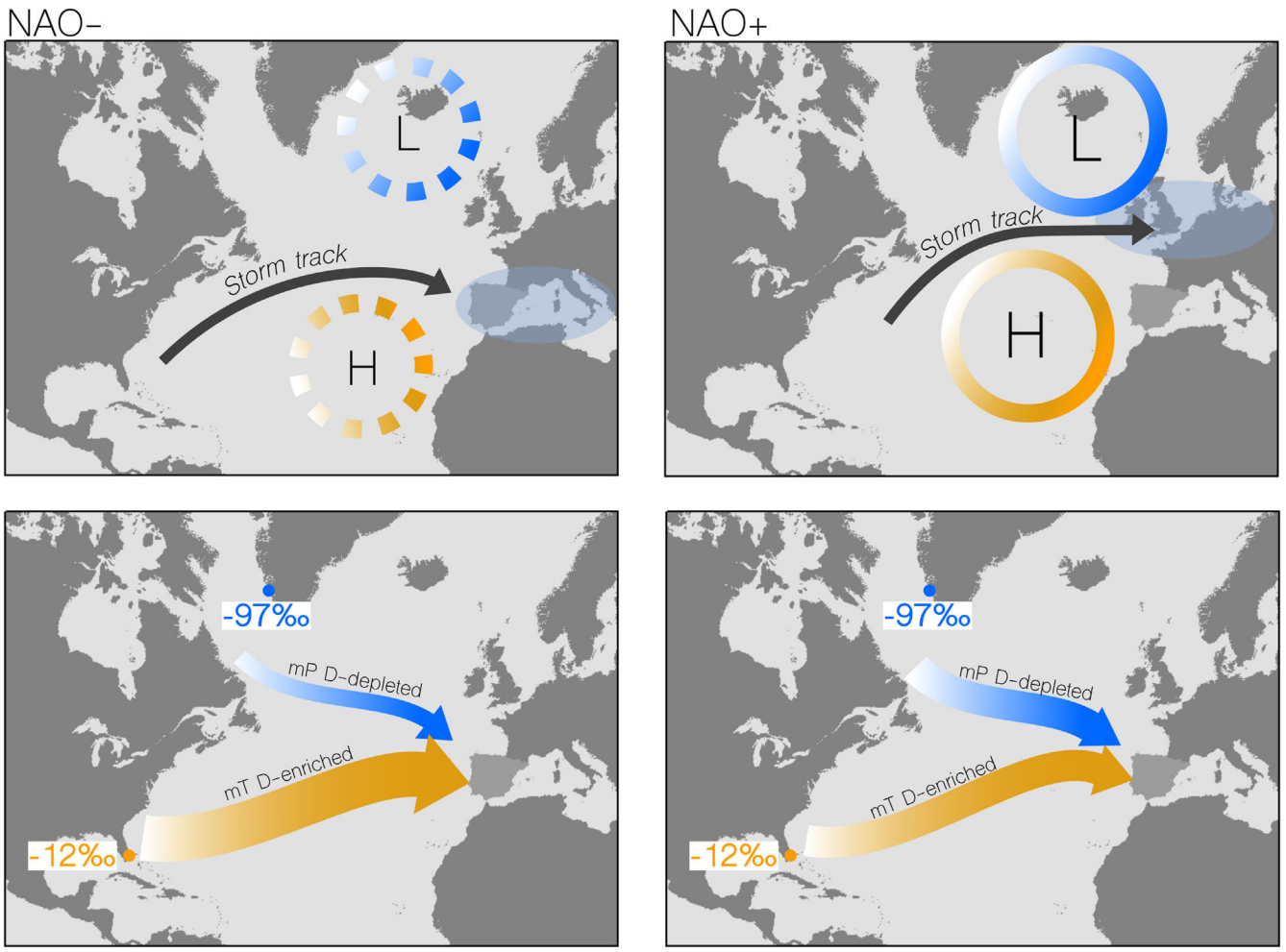

Figure 5. Winter atmospheric circulation during negative and positive modes of the NAO (top panels) and the corresponding proposed impact on moisture transport to the Iberian Peninsula (bottom panels). The dashed lines defining the Azores High and Icelandic Low indicate that these pressure systems are weaker, and arrow thickness in the bottom panels is representative of the relative magnitude of moisture delivery. Illustrative annual precipitation δD values in Paamiut, Greenland (−97‰) and Miami, Florida (−12‰) were estimated using the Online Isotopes in Precipitation Calculator (OIPC; Bowen and Revenaugh, 2003; IAEA/WMO, 2015; Bowen, 2017) and are indicated on the map.

Blood Pond in Massachusetts, and attributed this to differences in evapotranspiration related to microenvironment and potentially plant physiology or biochemistry. Species-specific fractionations further complicate paleoclimate interpretations of the δD_{wax} proxy, as changes in vegetation composition can contribute to temporal variability of sedimentary *n*-alkane δD.

Vegetation composition at PRC-South is highly variable, demonstrated by a range in P_{aq} of 0.787 (Fig. 3; Table S1), but these changes are dominantly driven by *Sphagnum* moss abundance. When changes in terrestrial vegetation composition are isolated using the Norm31 index (Fig. S3; Table S1), it is apparent that mid-chain *n*-alkanes derived from *Sphagnum* (C_{23} and C_{25}) are responsible for the substantial variations in P_{aq}. Norm31 values have a range of just 0.27 and generally vary minimally throughout the deposit (Fig. S3; Table S1). Relatively large changes in Norm31 occur between 6.4–6.3 and 5.7–5.6k cal a BP (Fig. S3; Table S1), but these fluctuations are probably inconsequential. *Sphagnum* peatlands are characterized by low vascular plant biodiversity that can help to reduce the effects of vegetation composition on sedimentary plant wax δD values (Nichols *et al.*, 2010) and terrestrial vegetation change is unlikely to have significantly influenced $\delta D_{n\text{-}C29}$ values at PRC-South. However, substantial fluctuations in mid-chain *n*-alkane origin due to the drastic reduction in *Sphagnum* potentially contributed to δD variability of *n*-C_{23}, *n*-C_{25} and *n*-C_{27}, which makes them unreliable for climatic reconstruction. This is likely reflected by the distinct trend divergence between mid-chain and long-chain *n*-alkane δD values (Fig. S1). Similarly, various *Sphagnum* mosses abundantly produce or maximize at *n*-C_{31} (Nichols *et al.*, 2006), and *n*-C_{31} is probably also susceptible to δD modifications as a result of origin variability in *Sphagnum* wetlands. For that reason, we solely interpret *n*-C_{29} for hydroclimatic purposes and do not consider vegetation composition to be a significant source of $\delta D_{n\text{-}C29}$ variability.

Temperature change is also considered in our hydroclimate reconstruction. In addition to moisture source, temperature is a dominant control on the isotopic composition of precipitation in Iberia (Carreira *et al.*, 2005). Temperature change during the relatively short period encompassed by the PRC-South deposit (6.6–5.4k cal a BP) is small, however, and regional sea surface temperatures gradually decrease by just ∼1 °C during this time (Martrat *et al.*, 2015). The $\delta D_{n\text{-}C29}$ values at PRC-South range over ∼54‰, and the temperature decrease alone cannot account for the large magnitude of change in $\delta D_{n\text{-}C29}$ values. We propose that the ultimate origin of change in $\delta D_{n\text{-}C29}$ values is moisture source, but we do consider the potential isotopic effects of temperature change in greater detail in relevant zones.

Implications of Iberian Peninsula moisture transport for the interpretation of prehistoric plant wax δD

During the wet season in Iberia, tropical moisture dominates regional precipitation (Gimeno *et al.*, 2010). The meridional transport of tropical water vapor to the Iberian Peninsula primarily occurs through corridors of moisture known as atmospheric rivers (Gimeno *et al.*, 2014), which are frequently responsible for extreme precipitation events in the region (Lavers and Villarini, 2013; Ramos *et al.*, 2015) and contribute to the development of explosive extra-tropical cyclones (Ferreira *et al.*, 2016). The trajectory of atmospheric rivers has been linked to the NAO, with negative (positive) phases resulting in atmospheric rivers and heavy precipitation over southern (northern) Europe (Lavers and Villarini, 2013). The compound-specific hydrogen isotope record at PRC-South likely represents a long enough period (>1 ka) for changes in precipitation source related to the NAO to be recorded in plant wax δD. Given that the transport of tropical moisture to Portugal is greatest during the winter (Gimeno *et al.*, 2010) when a negative phase of the NAO enhances storminess and precipitation in Iberia and favors the passage of atmospheric rivers through southern Europe (Hurrell *et al.*, 2001; Lavers and Villarini, 2013), positive $\delta D_{n\text{-}C29}$ excursions are likely attributable to a negative NAO. The northern diversion of atmospheric rivers and storm tracks during positive phases of the NAO (Lavers and Villarini, 2013) likely reduces the delivery of D-enriched tropical moisture to the Iberian Peninsula, thus resulting in relatively low precipitation and *n*-alkane δD values (Fig. 5). Despite the established relationship between the NAO and atmospheric river trajectories, no strong or significant correlation between phases of the NAO and precipitation δD at two sites in Portugal (Porto and Faro) is evident (Baldini *et al.*, 2008). We suspect this relationship would be better expressed over longer timescales and in lipid δD values, as they potentially provide a temporally integrated isotopic signature. Given that our interpretation of changes in precipitation δD in relation to the NAO is speculative, we attribute variations in plant wax δD values to phases of the NAO only in the presence of additional proxies of humidity and storminess that can help to further characterize atmospheric mechanisms of climate change.

Zone 1: 6.6–6.4k cal a BP

The establishment of *Sphagnum* moss at PRC-South, indicated by geochemical evidence (P_{aq} values >0.8 and C/N ratios of approximately 50; Fig. 3), is probably related to geomorphic change induced by the deceleration of sea level rise, but still implies humid conditions in the region. The predominance of *Sphagnum* indicates a relatively wet environment, and deposit minimum $\delta^{13}C_{n\text{-}C29}$ values further support a prevailing humid climate between approximately 6.6 and 6.5k cal a BP. More positive $\delta D_{n\text{-}C29}$ values in Zone 1 (Fig. 3) are probably reflective of enhanced tropical moisture transport to the peninsula and high sand content in this zone indicates greater eolian-induced sand movement or surface runoff likely related to Atlantic storminess. The sand content of coastal bogs and lakes is frequently used to characterize prehistoric eolian sand movement in relation to regional storminess (e.g. Björckl and Clemmensen, 2004; de Jong et al., 2006), and given PRC-South's location, we similarly utilize sand content to help elucidate mechanisms of Atlantic atmospheric circulation. Combined evidence of increased rainfall, southerly derived precipitation, and strengthened westerlies indicates a persistent negative phase of the NAO during wetland formation. In the Roñanzas peat bog in Asturias, Spain (Fig. 1), elevated P_{aq} and decreased average chain length (ACL) also support a prevailing negative phase of the NAO during this time (Ortiz *et al.*, 2010).

After 6.5k cal a BP, decreased, but moderate, $\delta D_{n\text{-}C29}$ values indicate a latitudinal shift in the westerlies and a consequent reduction in tropical moisture transport to the peninsula. Corresponding to this transition towards more intermediate $\delta D_{n\text{-}C29}$ values is a decrease in sand content by ~20% (Fig. 3) and a substantial loss of *Sphagnum*, reflected by a large reduction in mid-chain *n*-alkanes (~50%; Fig. 4) and decreased C/N (Fig. 3). P_{aq} displays a strong correspondence to $\delta D_{n\text{-}C29}$ values in Zone 1 (Fig. 3), indicating that a decline in precipitation resulting from altered atmospheric circulation likely led to the reduction in *Sphagnum* cover rather than any geomorphic change of the wetland. Although the shift in vegetation composition does represent a considerable change in climate, the hydrologic sensitivity of *Sphagnum* in this ecotonal region likely magnified the climatic signal, and the actual reduction in regional precipitation was not as drastic as it appears in the molecular record. A predominance of C_{31} *n*-alkanes during this period (Fig. 4) could be representative of an increased abundance of Ericaceae or Poaceae species (Pancost *et al.*, 2002; Kirkels *et al.*, 2013). Ericaceae, in particular, was dominant at PRC-North during MIS 5d–5a, with pollen percentages averaging ~30% and maximizing at >60% (Minckley *et al.*, 2015), and its predominance would further indicate a drier climate. This transition to less humid conditions is also indicated by an increase in $\delta^{13}C_{n\text{-}C29}$ values (Fig. 3). The increase is small (<2‰) and probably indicative of greater water stress in dominant C_3 taxa, such as Ericaceae, rather than an expansion of C_4 vegetation (Farquhar *et al.*, 1989). Together, decreased sand deposition, reduced precipitation, and reduced tropical moisture transport suggest a northward displacement of mid-Atlantic storm tracks resulting from a dominantly positive phase of the NAO.

Zone 2: 6.4–5.9k cal a BP

We interpret the intermediate $\delta D_{n\text{-}C29}$ values and reduced sand content from 6.4 to 5.9k cal a BP to represent a sustained mixed moisture source and a prolonged positive phase of the NAO (Fig. 3). Sediments in this zone are primarily composed of organic matter, which probably indicates geomorphic stability (decreased eolian sand influx) because of reduced storminess. P_{aq} values indicate minor changes in precipitation and alternations of dominant vegetation communities (*Sphagnum vs.* terrestrial). A predominance of $n\text{-}C_{25}$ (Fig. 4) and higher P_{aq} values (Fig. 3) at 6.3, 6.2, and 5.9k cal a BP indicate that comparatively humid phases probably punctuated this drier period. Despite considerable sand content at 6.4 and 6.1k cal a BP, which may be interpreted as greater wind intensity and increased precipitation, a drier environment is indicated by decreased P_{aq} and predominance of the $n\text{-}C_{31}$ alkane, which is probably representative of a terrestrial replacement of *Sphagnum* moss at PRC-South. These intermittent dry phases may have been characterized by stronger, but less frequent, storms that promoted interspersed erosion and enhanced sediment mobility. Alternatively, increased sand content during these periods could be a consequence of a drier environment, as dry sand is more easily transported and vegetation loss could have exposed more sediment for erosion.

Zone 3: 5.9–5.4k cal a BP

A reorganization of atmospheric circulation over the Atlantic and a period of increased storm frequency and/or intensity in coastal Iberia is apparent between 5.9 and 5.4k cal a BP at PRC-South. A progression towards more negative $\delta D_{n\text{-}C29}$ values and corresponding sand invasion indicate an enhanced transport of high-latitude, D-depleted moisture to the region and a gradual intensification of westerly winds. In the Roñanzas peat bog in northern Spain, molecular markers indicate that this was a humid period and *Sphagnum* predominated (Ortiz *et al.*, 2010). At PRC-South, molecular distributions of *n*-alkanes demonstrate greater terrestrial plant growth, indicating that although this period was stormy in central Portugal, it was not necessarily associated with increased precipitation. Alternatively, vegetation feedbacks initiated by earlier, substantial *Sphagnum* loss may have contributed to increased interspecific competition, preventing local *Sphagnum* resilience. *Sphagnum* mosses limit vascular plant growth through nutrient interception and the formation of acidic, anoxic conditions, thus *Sphagnum* decline has the potential to increase nutrient availability, decomposition, and terrestrial development in wetland ecosystems (van Breemen, 1995; Malmer *et al.*, 2003). Reduced *Sphagnum* cover at PRC-South corresponds with significant decreases in sedimentary C/N (Fig. 3), suggesting that *Sphagnum* loss did alter biogeochemical processes to some extent. If increased precipitation accompanied greater nutrient cycling, expansion of terrestrial vegetation could have contributed to the absence of *Sphagnum* predominance despite a return to ideal climatic conditions for *Sphagnum* growth. However, $\delta^{13}C_{n\text{-}C29}$ values in this zone do not return to pre-*Sphagnum* decline values, and this was likely a comparatively dry period at PRC-South.

Polar control on Iberian hydroclimate and storminess

The environmental and climatic transition apparent in Zone 3 (5.9–5.4k cal a BP) can be attributed to a decline in North Atlantic sea surface temperatures (SSTs), which suppressed tropical moisture sources and exerted a stronger polar climatic influence on the region and much of Europe. A series of these SST cooling episodes, often referred to as Bond events, have occurred throughout the Holocene and are attributed to changes in solar irradiance (Bond *et al.*, 2001). The effects of Bond events are especially evident in the North Atlantic and have been identified using changes in ice-rafted debris (IRD) found in deep-sea sediment cores from the North Atlantic basin (Bond *et al.*, 1997). The period encompassed in the PRC-South organic deposit coincides with Bond Event 4 (Fig. 6), associated with extended sea ice cover and global glacial advances (Mayewski *et al.*, 2004). The extra-regional impacts of Bond Event 4 are typically apparent in proxy records starting at approximately 6 ka (Mayewski *et al.*, 2004; Fletcher and Zielhofer, 2013), and are similarly evident at PRC-South. In Zone 3, between 5.9 and 5.4k cal a BP, $\delta D_{n\text{-}C29}$ values display a strong correspondence to IRD of Bond Event 4, implying a significant North Atlantic SST control on precipitation source in Iberia (Fig. 6). The apparent lag in response to North Atlantic climate during Bond Event 4, which begins at ~6.6 ka, is probably related to the initial small magnitude of change and significant latitudinal separation between PRC-South and the origin of SST cooling. Similarly, the large fluctuations in Zone 3 $\delta D_{n\text{-}C29}$ values associated with relatively minimal changes in IRD are likely representative of Portugal's location at the southernmost extent of North Atlantic influence and its sensitivity to small variations in moisture trajectory.

Although depressed North Atlantic SSTs probably also contributed to more negative precipitation δD and resultant $\delta D_{n\text{-}C29}$ values, the relatively small estimated SST change (<2 °C; Bond *et al.*, 1997; Rodrigues *et al.*, 2009) cannot account for most of the ~52‰ decrease in $\delta D_{n\text{-}C29}$ values that occurred during this event. Across a 7° latitudinal transect off the Iberian coast, equating to an approximate 2 °C SST difference, the surface δD of seawater ranges just 4‰ (Voelker *et al.*, 2015). Similarly, a lower condensation temperature may also have influenced precipitation δD. However, given that an average annual temperature range of ~10 °C results in a relatively small range of 16‰ in monthly averaged meteoric δD values at PRC, atmospheric temperature changes probably also contributed minimally to $\delta D_{n\text{-}C29}$ variability and the large magnitude of change in $\delta D_{n\text{-}C29}$ values primarily reflects enhanced polar moisture transport to the peninsula.

Between 5.9 and 5.4k cal a BP, considerable changes in sand content at PRC-South also correspond with shifts in $\delta D_{n\text{-}C29}$ values (Fig. 3), representing a likely link between progressive cooling, regional storminess, and dune emplacement. The end of the deposit (~5.4k cal a BP) coincides with peak IRD during Bond Event 4, high sand content in the PRC-South outcrop (97%), and the lowest $\delta D_{n\text{-}C29}$ values, indicating that powerful storms likely led to the ultimate burial of the wetland (Fig. 3; Fig. 6). Sand movement and coastal dune migration at other sites in Iberia (Fig. 1) are consistent with the timing at PRC-South. These include a storm deposit dated to 5.7 ka in the Odiel estuary in southwestern Spain (Ruiz *et al.*, 2007), a period of storm-induced dune activity around 5.6 ka at Caparica near Lisbon (Costas *et al.*, 2012), and sand invasion of a coastal lagoon resulting from a high-energy storm or tsunami event between 5.4 and 5.2 ka at Doñana National Park (Ruiz *et al.*, 2005). Enhanced storm activity also characterizes the period between 5.7 and 5.4 ka in the Gulf of Lions along the French Mediterranean coast (Sabatier *et al.*, 2012). Although Holocene sea level rise probably

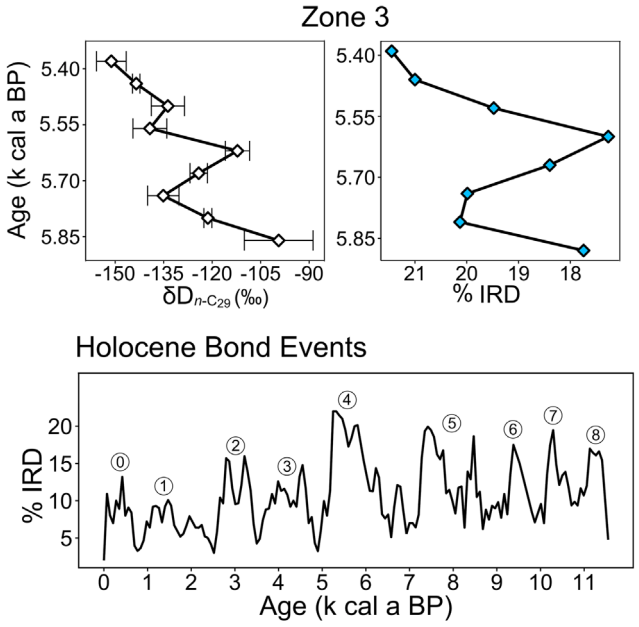

Figure 6. Comparison between Zone 3 $\delta D_{n\text{-}C29}$ at PRC-South and % IRD (hematite-stained grains) during Bond Event 4 (Bond *et al.*, 2001). All Bond events throughout the Holocene are displayed as % hematite-stained grains in the bottom right panel (Bond *et al.*, 2001).

contributed to coastal instability and sediment supply in these and other locations, a strong correspondence between Bond Event 4, coastal storms, and dune encroachment suggests a primarily climatic control on sand movement (Costas *et al.*, 2012).

Atmospheric response of the NAO to North Atlantic climate change

During Bond Event 4, storminess combined with an inferred high-latitude origin of precipitation at PRC-South likely demonstrates a reorganization of the NAO because of North Atlantic climate change. Enhanced westerly winds over the peninsula and consequent sand mobility are typically associated with a negative NAO and, as we have proposed, greater tropical moisture transport to Iberia. However, strong storms from 5.9 to 5.4k cal a BP instead coincide with a D-depleted precipitation source at PRC-South, a moisture trajectory that is perhaps more characteristic of a positive phase of the NAO. Irregular NAO behavior during peak cooling of Bond Event 4 is further evidenced by concurrent dune formation in northern Europe (Costas *et al.*, 2012). Under a conventional NAO atmospheric arrangement, dune building does not occur simultaneously along the entirety of the European coast due to the westerlies primarily tracking north or south in positive or negative NAO phases, respectively (Clarke and Rendell, 2006). Therefore, synchronous sand drift in Iberia and northern Europe implies that an alternative mechanism of westerly flow was established during this cold event.

Periods of enhanced European storminess throughout the Holocene frequently coincide with multi-decadal cold events (Costas *et al.*, 2012; Sabatier *et al.*, 2012; Degeai *et al.*, 2015), of which the most recognized is the Little Ice Age (LIA). The LIA is marked by synchronous storm activity along the European coast and contradictory records of the NAO (Trouet *et al.*, 2012), similar to Bond Event 4. Storminess during the LIA and other Holocene cold events is typically attributed to solar irradiance (Bond *et al.*, 2001; Degeai *et al.*, 2015) or internal ocean–atmosphere variability (Sorrel *et al.*, 2012; Trouet *et al.*, 2012). Based on climate model simulations, Trouet *et al.* (2012) discuss a probable weakening of the Atlantic Meridional Overturning Circulation that contributed to a negative NAO atmospheric arrangement and cool climatic conditions during the LIA. Additionally, Trouet *et al.* (2012) attribute proxy evidence of synchronous storminess to increased storm intensity, not frequency, and limitations of storminess proxies, such as the inability to differentiate storm occurrence by season. Wirth and Sessions (2016) present compound-specific hydrogen isotope evidence of enhanced tropical moisture transport to the Mediterranean region that further supports a likely negative phase of the NAO during the LIA. Synchronous storminess during Bond Event 4 could certainly reflect more frequent summer storms or enhanced storm intensity. However, a negative NAO atmospheric arrangement similar to that of the LIA is not consistent with the PRC-South record of increasingly polar-derived precipitation and relatively dry climatic conditions in coastal Portugal. Costas *et al.* (2012, 2016) suggest an intensification of westerly zonal winds resulting from a stronger latitudinal temperature gradient across the Atlantic and a southward displacement and deepening of the Icelandic low during Bond Event 4 (Fig. 7). This mechanism would permit strong westerly winds along the entirety of the European coastline and also support the southward extension of polar, D-depleted moisture transport that is evidenced by the near 52‰ decrease in $\delta D_{n\text{-}C29}$ values at PRC-South. Altered

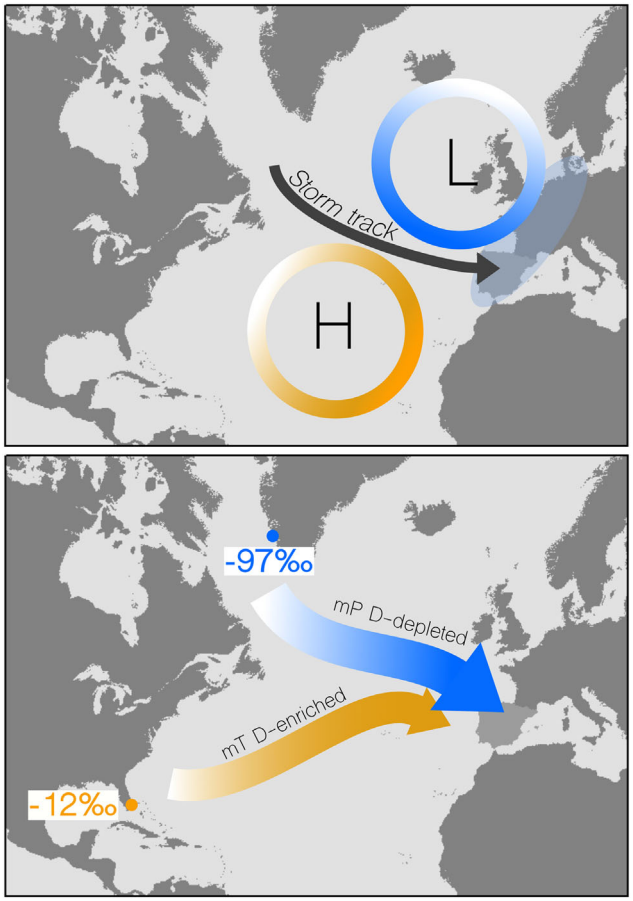

Figure 7. Proposed mechanism of winter atmospheric circulation between 5.9 and 5.4 ka (Costas *et al.*, 2012, 2016). The top panel displays the effect of a displaced and strong Icelandic Low on mid-latitude storm-tracks, and the bottom displays the resultant increase in D-depleted moisture transport to Iberia. The dashed lines defining the Azores High and Icelandic Low indicate that these pressure systems are weaker, and arrow thickness in the bottom panel is representative of the relative magnitude of moisture delivery. Illustrative annual precipitation δD values in Paamiut, Greenland (−97‰) and Miami, Florida (−12‰) were estimated using the Online Isotopes in Precipitation Calculator (OIPC; Bowen and Revenaugh, 2003; IAEA/WMO, 2015; Bowen, 2017) and are indicated on the map.

'centers of action' of the NAO resulting from the climate-induced displacement of the Icelandic low could have allowed for modified moisture transport and the regional synchronicity of storminess that is atypical of the more pervasive Holocene mechanism of NAO. Further investigations into atmospheric rearrangements during Holocene cold events are necessary to assess the predictability of the NAO's response to North Atlantic cooling and whether a consistent forcing mechanism is responsible for atmospheric circulation variability during these events.

Conclusions

The molecular and isotopic record at PRC-South presents valuable evidence of environmental and climatic change on a relatively short timescale (6.6–5.4k cal a BP). From 6.6 to 6.5k cal a BP, the PRC-South wetland formed during a brief humid interval that supported the dominance of *Sphagnum* moss and peat formation. A prominently tropical source of precipitation is indicated by more positive $\delta D_{n\text{-}C29}$ values, and a negative NAO phase probably prevailed. A subsequent dry period lasting from 6.5 to 5.9k cal a BP resulted in a substantial *Sphagnum* decline, which is marked by significant

changes in P_{aq} and C/N ratios. The initial predominance of a localized *Sphagnum* population and subsequent decline because of reduced precipitation is exemplary of PRC's vulnerable, transitional location between Atlantic and Mediterranean bioclimatic regimes. Intermediate $\delta D_{n\text{-}C29}$ values representing a more mixed moisture source and geomorphic stability during this period suggest a transition to a positive phase of the NAO was responsible for the reduction in precipitation.

From 5.9 to 5.4k cal a BP, a pronounced North Atlantic climatic control is responsible for more negative $\delta D_{n\text{-}C29}$ values and regional storminess. Cooling associated with Bond Event 4 likely resulted in a displaced Icelandic low and strengthened zonal westerlies (Costas *et al.*, 2012, 2016), which extended the transport of northerly derived precipitation to southern Europe. Consequent storminess led to dune encroachment in northern Europe and along the Iberian coast, eventually burying the PRC-South wetland at the height of North Atlantic cooling. The climatic record of this interval especially emphasizes the sensitivity of Iberian precipitation regimes and mid-latitude storm tracks to North Atlantic climate change and the vulnerability of coastal environments to storminess and sand invasion. In the future, the North Atlantic region will likely be subjected to amplified warming (Overland *et al.*, 2014) and the consequent changes in atmospheric and oceanic circulation could significantly impact the hydroclimatology and ecology of the Iberian Peninsula, especially the ecotonal Estremadura region.

Compound-specific hydrogen isotope analysis has yet to be fully utilized as a proxy for prehistoric changes in European moisture transport, with few exceptions (e.g. Schemmel *et al.*, 2016; Wirth and Sessions, 2016). Although the paleoclimate record presented here encompasses just 1200 years, it demonstrates the significant potential of multi-proxy reconstructions, which include compound-specific hydrogen isotopes, to better understand complex atmospheric reorganizations and the resulting hydrologic repercussions. Given greater research into the controls of climatic oscillations on precipitation source and δD, the application of compound-specific hydrogen isotope analysis to carefully selected sites along the European coast could provide valuable insight into the long-term atmospheric dynamics of the NAO.

Supplementary information

Figure S1. Compound-specific δD values for each odd-numbered *n*-alkane (C_{23}–C_{33}) at 10-cm intervals throughout the PRC-South deposit. Stratigraphic zones 1, 2 and 3 are indicated on the right.

Figure S2. Compound-specific $\delta^{13}C$ values for each odd-numbered *n*-alkane (C_{23}–C_{33}) throughout the PRC-South deposit. Stratigraphic zones are indicated by 1, 2 and 3 on the right.

Figure S3. PRC-South Norm31 and carbon preference index (CPI) results. Stratigraphic zones are indicated by 1, 2 and 3 on the right.

Acknowledgements. Fieldwork in Portugal was funded by the US National Science Foundation, Archeology Program (BCS-1118183 and BCS-1420453) and funding support for instrumental analysis was provided by NSF EAR-1427494 and the UNCW Center for Marine Science. Additional funding was provided by the UNCW Center for the Support of Undergraduate Research and Fellowships. We would also like to thank Forrest Melvin for assistance with sedimentary analyses and the student crew who assisted with sampling in 2013. We appreciate the comments and suggestions from two anonymous reviewers, which greatly improved the quality and strength of the manuscript.

Abbreviations. CPI, carbon preference index; DCM, dichloromethane; IRD, ice-rafted debris; LIA, Little Ice Age; MIS, Marine Isotope Stage; NAO, North Atlantic Oscillation; OSL, optically stimulated luminescence; PRC, Praia Rei Cortiço; SST, sea surface temperature.

References

Andersson RA, Kuhry P, Meyers P *et al.* 2011. Impacts of paleohydrological changes on *n*-alkane biomarker compositions of a Holocene peat sequence in the eastern European Russian Arctic. *Organic Geochemistry* **42**: 1065–1075.

Araguás Araguás LJ, Diaz Teijeiro MF. 2005. Isotope composition of precipitation and water vapour in the Iberian Peninsula. First results of the Spanish network of isotopes in precipitation. In *Isotopic Composition of Precipitation in the Mediterranean Basin in Relation to Air Circulation Patterns and Climate*. IAEA: Vienna; 173–190.

Baas M, Pancost R, van Geel B *et al.* 2000. A comparative study of lipids in Sphagnum species. *Organic Geochemistry* **31**: 535–541.

Baldini LM, McDermott F, Foley AM *et al.* 2008. Spatial variability in the European winter precipitation $\delta^{18}O$-NAO relationship: Implications for reconstructing NAO-mode climate variability in the Holocene. *Geophysical Research Letters* **35**: L04709.

Bao R, Alonso A, Delgado C *et al.* 2007. Identification of the main driving mechanisms in the evolution of a small coastal wetland (Traba, Galicia, NW Spain) since its origin 5700 cal yr BP. *Palaeogeography, Palaeoclimatology, Palaeoecology* **247**: 296–312.

Benedetti MM, Haws JA, Funk CL *et al.* 2009. Late Pleistocene raised beaches of coastal Estremadura, central Portugal. *Quaternary Science Reviews* **28**: 3428–3447.

Bi XH, Sheng GY, Liu XH *et al.* 2005. Molecular and carbon and hydrogen isotopic composition of *n*-alkanes in plant leaf waxes. *Organic Geochemistry* **36**: 1405–1417.

Bingham EM, McClymont EL, Väliranta M *et al.* 2010. Conservative composition of *n*-alkane biomarkers in Sphagnum species: implications for palaeoclimate reconstruction in ombrotrophic peat bogs. *Organic Geochemistry* **41**: 214–220.

Björckl S, Clemmensen LB. 2004. Aeolian sediment in raised bog deposits, Halland, SW Sweden: a new proxy record of Holocene winter storminess variation in southern Scandinavia? *Holocene* **14**: 677–688.

Blaauw M. 2010. Methods and code for 'classical' age-modelling of radiocarbon sequences. *Quaternary Geochronology* **5**: 512–518

Bond G, Kromer B, Beer J *et al.* 2001. Persistent solar influence on North Atlantic climate during the Holocene. *Science* **294**: 2130–2136.

Bond G, Showers W, Cheseby M *et al.* 1997. A pervasive millennial-scale cycle in North Atlantic Holocene and glacial climates. *Science* **278**: 1257–1266.

Boski T, Moura D, Veiga-Pires C *et al.* 2002. Postglacial sea-level rise and sedimentary response in the Guadiana Estuary, Portugal–Spain border. *Sedimentary Geology* **150**: 103–122.

Bowen GJ. 2017. *The Online Isotopes in Precipitation Calculator, version 3.1*. www.waterisotopes.org.

Bowen GJ, Revenaugh J. 2003. Interpolating the isotopic composition of modern meteoric precipitation. *Water Resources Research* **39**.

Carr AS, Boom A, Grimes HL *et al.* 2014. Leaf wax *n*-alkane distributions in arid zone South African flora: environmental controls, chemotaxonomy and palaeoecological implications. *Organic Geochemistry* **67**: 72–84.

Carreira PMM, Araujo MF, Nunes D. 2005. Isotopic composition of rain and water vapour samples from Lisbon region: characterization of monthly and daily events. In *Isotopic Composition of Precipitation in the Mediterranean Basin in Relation to Air Circulation Patterns and Climate*. IAEA: Vienna 141–155.

Clarke ML, Rendell HM. 2006. Effects of storminess, sand supply and the North Atlantic Oscillation on sand invasion and coastal dune accretion in western Portugal. *Holocene* **16**: 341–355.

Clarke ML, Rendell HM. 2009. The impact of North Atlantic storminess on Western European coasts: a review. *Quaternary International* **195**: 31–41.

Corona MG, Vicente AM, Novo FG. 1988. Long-term vegetation changes on the stabilized dunes of Donana-National-Park (SW Spain). *Vegetatio* **75**: 73–80.

Costa JC, Lousã M, Capelo J *et al.* 2000. The coastal vegetation of the Portuguese Divisory Sector: Dunes cliffs and lowscrub communities. *Finisterra* **35**: 69–93.

Costas S, Jerez S, Trigo RM *et al.* 2012. Sand invasion along the Portuguese coast forced by westerly shifts during cold climate events. *Quaternary Science Reviews* **42**: 15–28.

Costas S, Naughton F, Goble R *et al.* 2016. Windiness spells in SW Europe since the last glacial maximum. *Earth and Planetary Science Letters* **436**: 82–92.

Danielsen R, Castilho AM, Dinis PA *et al.* 2012. Holocene interplay between a dune field and coastal lakes in the Quiaios-Tocha region, central littoral Portugal. *Holocene* **22**: 383–395.

Dansgaard W. 1964. Stable isotopes in precipitation. *Tellus* **16**: 436–468.

de Carvalho GS, Granja HM, Loureiro E *et al.* 2006. Late Pleistocene and Holocene environmental changes in the coastal zone of northwestern Portugal. *Journal of Quaternary Science* **21**: 859–877.

de Jong R, Björk S, Björkman L, Clemmensen LB. 2006. Storminess variation during the last 6500 years as reconstructed from an ombrotrophic peat bog in Holland, southwest Sweden. *Journal of Quaternary Science* **21**: 905–919.

Degeai JP, Devillers B, Dezileau L, Oueslati H, Bony G. 2015. Major storm periods and climate forcing in the Western Mediterranean during the Late Holocene. *Quaternary Science Reviews* **129**: 37–56.

Eglinton TI, Eglinton G. 2008. Molecular proxies for paleoclimatology. *Earth and Planetary Science Letters* **275**: 1–16.

Farquhar GD, Ehleringer JR, Hubick KT. 1989. Carbon isotope discrimination and photosynthesis. *Annual Review of Plant Physiology and Plant Molecular Biology* **40**: 503–537.

Ferreira JA, Liberato MLR, Ramos AM. 2016. On the relationship between atmospheric water vapour transport and extra-tropical cyclones development. *Physics and Chemistry of the Earth* **94**: 56–65.

Ficken KJ, Li B, Swain DL *et al.* 2000. An n-alkane proxy for the sedimentary input of submerged/floating freshwater aquatic macrophytes. *Organic Geochemistry* **31**: 745–749.

Fischer H, Mieding B. 2005. A 1,000-year ice core record of interannual to multidecadal variations in atmospheric circulation over the North Atlantic. *Climate Dynamics* **25**: 65–74.

Fletcher WJ, Zielhofer C. 2013. Fragility of western Mediterranean landscapes during Holocene rapid climate changes. *Catena* **103**: 16–29.

Freitas MC, Andrade C, Cruces A. 2002. The geological record of environmental changes in southwestern Portuguese coastal lagoons since the Lateglacial. *Quaternary International* **93–94**: 161–170.

Galimov E. 1985. Isotopic composition of the carbon of organisms. In *The Biological Fractionation of Isotopes*, Galimov E (ed.). Academic Press, Inc.: New York; 16–38.

Gimeno L, Nieto R, Trigo RM *et al.* 2010. Where does the Iberian Peninsula moisture come from? An answer based on a Lagrangian approach. *Journal of Hydrometeorology* **11**: 421–436

Gimeno L, Nieto R, Vazquez M *et al.* 2014. Atmospheric rivers: a mini-review. *Frontiers in Earth Science* **2**.

Giorgi F 2006. Climate change hot-spots. *Geophysical Research Letters* **33**: L08707.

Giorgi F, Lionello P. 2008. Climate change projections for the Mediterranean region. *Global and Planetary Change* **63**: 90–104.

González-Villanueva R, Pérez-Arlucea M, Costas S *et al.* 2015. 8000 years of environmental evolution of barrier-lagoon systems emplaced in coastal embayments (NW Iberia). *Holocene* **25**: 1786–1801.

Granja H, Monteiro-Rodrigues S, Danielsen R. 2016. Changing environments and human settlement during Mid-Holocene in Rio de Moinhos beach (Esposende, Northern Portgual). *Estudos do Quaternário* **14**: 25–40.

Haws JA, Benedetti MM, Funk CL *et al.* 2010. Coastal wetlands and the Neanderthal settlement of Portuguese Estremadura. *Geoarchaeology* **25**: 709–744.

Heiri O, Lotter AF, Lemcke G. 2001. Loss on ignition as a method for estimating organic and carbonate content in sediments: reproducibility and comparability of results. *Journal of Paleolimnology* **25**: 101–110.

Hou J, D'Andrea WJ, MacDonald D *et al.* 2007. Hydrogen isotopic variability in leaf waxes among terrestrial and aquatic plants around Blood Pond, Massachusetts (USA). *Organic Geochemistry* **38**: 977–984.

Hurrell JW, Kushnir Y, Visbeck M. 2001. Climate. The North Atlantic oscillation. *Science* **291**: 603–605.

IAEA/WMO. 2015. Global Network of Isotopes in Precipitation. The GNIP Database. Accessible at: https://nucleus.iaea.org/wiser.

Jain M, Bøtter-Jensen L, Singhvi AK. 2003. Dose evaluation using multiple-aliquot quartz OSL: test of methods and a new protocol for improved accuracy and precision. *Radiation Measurements* **37**: 67–80.

Kirkels FMSA, Jansen B, Kalbitz K. 2013. Consistency of plant-specific *n*-alkane patterns in Plaggen ecosystems: a review. *Holocene* **23**: 1355–1368.

Lane CS, Horn SP, Kerr MT. 2014. Beyond the Mayan lowlands: impacts of the terminal classic drought in the Caribbean Antilles. *Quaternary Science Reviews* **86**: 89–98.

Lavers DA, Villarini G. 2013. The nexus between atmospheric rivers and extreme precipitation across Europe. *Geophysical Research Letters* **40**: 3259–3264.

Lionello P, Abrantes F, Congedi L *et al.* 2012. Introduction: Mediterranean climate-background information. In *Climate of the Mediterranean Region: from the Past to the Future*, Lionello P (ed.). Elsevier: London xxxv-lxxx.

Malmer N, Albinsson C, Svensson BM *et al.* 2003. Interferences between *Sphagnum* and vascular plants: effects on plant community structure and peat formation. *Oikos* **100**: 469–482.

Marshall J, Kushnir Y, Battisti D *et al.* 2001. North Atlantic climate variability: phenomena, impacts and mechanisms. *International Journal of Climatology* **21**: 1863–1898.

Martrat B, Tzedakis PC, Margari V *et al.* 2015. Multi-decadal temperature changes off Iberia over the last two deglaciations and interglacials and their connection with the polar climate. *Past Global Changes Magazine* **23**: 10–11.

Marzi R, Torkelson BE, Olson RK. 1993. A revised carbon preference index. *Organic Geochemistry* **20**: 1303–1306.

Mayewski PA, Rohling EE, Curt Stager JC *et al.* 2004. Holocene climate variability. *Quaternary Research* **62**: 243–255.

Minckley TA, Haws JA, Benedetti MM *et al.* 2015. Last interglacial vegetation and climate history from the Portuguese coast. *Journal of Quaternary Science* **30**: 59–69.

Moossen H, Bendle J, Seki O *et al.* 2015. North Atlantic Holocene climate evolution recorded by high-resolution terrestrial and marine biomarker records. *Quaternary Science Reviews* **129**: 111–127.

Muñoz-Reinoso JC. 2001. Vegetation changes and groundwater abstraction in SW Doñana, Spain. *Journal of Hydrology* **242**: 197–209.

Nichols J, Booth RK, Jackson ST *et al.* 2010. Differential hydrogen isotopic ratios of Sphagnum and vascular plant biomarkers in ombrotrophic peatlands as a quantitative proxy for precipitation—evaporation balance. *Geochimica et Cosmochimica Acta* **74**: 1407–1416.

Nichols JE, Booth RK, Jackson ST *et al.* 2006. Paleohydrologic reconstruction based on *n*-alkane distributions in ombrotrophic peat. *Organic Geochemistry* **37**: 1505–1513.

Nott CJ, Xie SC, Avsejs LA *et al.* 2000. *n*-Alkane distributions in ombrotrophic mires as indicators of vegetation change related to climatic variation. *Organic Geochemistry* **31**: 231–235.

Ortiz JE, Gallego JLR, Torres T *et al.* 2010. Palaeoenvironmental reconstruction of Northern Spain during the last 8000 cal yr BP based on the biomarker content of the Ronanzas peat bog (Asturias). *Organic Geochemistry* **41**: 454–466.

Overland JE, Wang M, Walsh JE *et al.* 2014. Future Arctic climate changes: adaptation and mitigation time scales. *Earth's Future* **2**: 68–74.

Pancost RD, Baas M, van Geel B *et al.* 2002. Biomarkers as proxies for plant inputs to peats: an example from a sub-boreal ombrotrophic bog. *Organic Geochemistry* **33**: 675–690.

Polissar PJ, D'Andrea WJ. 2014. Uncertainty in paleohydrologic reconstructions from molecular delta D values. *Geochimica et Cosmochimica Acta* **129**: 146–156.

Prescott JR, Hutton JT. 1994. Cosmic ray contributions to dose rates for luminescence and ESR dating: large depths and long-term time variations. *Radiation Measurements* **23**: 497–500.

Proctor CJ, Baker A, Barnes WL *et al.* 2000. A thousand year speleothem proxy record of North Atlantic climate from Scotland. *Climate Dynamics* **16**: 815–820.

Ramos AM, Trigo RM, Liberato MLR *et al.* 2015. Daily precipitation extreme events in the Iberian Peninsula and its association with atmospheric rivers. *Journal of Hydrometeorology* **16**: 579–597.

Rebeiro H, Bernal A, Flores D *et al.* 2011. A multidisciplinary study of an organic-rich mudstone in the Middle Holocene on the Northern coast of Portugal. *Comunicações Geológicas* **98**: 93–98.

Reimer PJ, Bard E, Bayliss A *et al.* 2013. IntCal13 and Marine13 radiocarbon age calibration curves 0-50,000 years cal BP. *Radiocarbon* **55**: 1869–1887.

Rodrigues T, Grimalt JO, Abrantes FG *et al.* 2009. Holocene interdependences of changes in sea surface temperature, productivity, and fluvial inputs in the Iberian continental shelf (Tagus mud patch). *Geochemistry, Geophysics, Geosystems* **10**: DOI: 10.1029/2008GC002367.

Ruiz F, Borrego J, López-González N *et al.* 2007. The geological record of a mid-Holocene marine storm in southwestern Spain. *Geobios* **40**: 689–699.

Ruiz F, Rodríguez-Ramírez A, Cáceres LM *et al.* 2005. Evidence of high-energy events in the geological record: mid-Holocene evolution of the southwestern Donana National Park (SW Spain). *Palaeogeography, Palaeoclimatology, Palaeoecology* **229**: 212–229.

Sabatier P, Dezileau L, Colin C *et al.* 2012. 7000 years of paleostorm activity in the NW Mediterranean Sea in response to Holocene climate events. *Quaternary Research* **77**: 1–11.

Sachse D, Billault I, Bowen GJ *et al.* 2012. Molecular paleohydrology: interpreting the hydrogen- isotopic composition of lipid biomarkers from photosynthesizing organisms. *Annual Review of Earth and Planetary Sciences* **40**: 221–249.

Sachse D, Radke J, Gleixner G. 2004. Hydrogen isotope ratios of recent lacustrine sedimentary *n*-alkanes record modern climate variability. *Geochimica et Cosmochimica Acta* **68**: 4877–4889.

Schemmel F, Niedermeyer EM, Schwab VF *et al.* 2016. Plant wax δD values record changing Eastern Mediterranean atmospheric circulation patterns during the 8.2 kyr B.P. climatic event. *Quaternary Science Reviews* **133**: 96–107.

Seneca A. 2003. The genus *Sphagnum* L. in Portugal. *Cryptogamie Bryologie* **24**: 103–126.

Smith AC, Wynn PM, Barker PA *et al.* 2016. North Atlantic forcing of moisture delivery to Europe throughout the Holocene. *Scientific Reports* **6**: 24745.

Sorrel P, Debret M, Billeaud I *et al.* 2012. Persistent non-solar forcing of Holocene storm dynamics in coastal sedimentary archives. *Nature Geoscience* **5**: 892–896.

Sousa A, Morales J, García-Barrón L *et al.* 2013. Changes in the *Erica ciliaris* Loefl. ex L. peat bogs of southwestern Europe from the 17th to the 20th centuries AD. *Holocene* **23**: 255–269.

Tierney JE, Russell JM, Sinninghe Damsté JS *et al.* 2011. Late Quaternary behavior of the East African monsoon and the importance of the Congo Air Boundary. *Quaternary Science Reviews* **30**: 798–807.

Tipple BJ, Pagani M. 2010. A 35Myr North American leaf-wax compound-specific carbon and hydrogen isotope record: implications for C4 grasslands and hydrologic cycle dynamics. *Earth and Planetary Science Letters* **299**: 250–262.

Trigo R, Xoplaki E, Zorita E *et al.* 2006. Relations between variability in the Mediterranean region and mid-latitude variability. In *Mediterranean Climate Variability*, Lionello P, Malanotte-Rizzoli P, Boscolo R (eds). Elsevier: Amsterdam 179–226.

Trigo RM, Osborn TJ, Corte-Real JM. 2002. The North Atlantic Oscillation influence on Europe: climate impacts and associated physical mechanisms. *Climate Research* **20**: 9–17.

Trouet V, Esper J, Graham NE *et al.* 2009. Persistent positive North Atlantic Oscillation mode dominated the Medieval Climate Anomaly. *Science* **324**: 78–80.

Trouet V, Scourse JD, Raible CC. 2012. North Atlantic storminess and Atlantic Meridional Overturning Circulation during the last Millennium: reconciling contradictory proxy records of NAO variability. *Global and Planetary Change* **84–85**: 48–55.

van Breemen N. 1995. How *Sphagnum* bogs down other plants. *Trends in Ecology and Evolution* **10**: 270–275.

Vis GJ, Kasse C, Vandenberghe J. 2008. Late Pleistocene and Holocene palaeogeography of the Lower Tagus Valley (Portugal): effects of relative sea level, valley morphology and sediment supply. *Quaternary Science Reviews* **27**: 1682–1709.

Visbeck MH, Hurrell JW, Polvani L *et al.* 2001. The North Atlantic Oscillation: past, present, and future. *Proceedings of the National Academy of Sciences of the United States of America* **98**: 12876–12877.

Voelker AHL, Colman A, Olack G *et al.* 2015. Oxygen and hydrogen isotope signatures of northeast Atlantic water masses. *Deep Sea Research Part II: Topical Studies in Oceanography* **116**: 89–106.

Wirth SB, Sessions AL. 2016. Plant-wax D/H ratios in the southern European Alps record multiple aspects of climate variability. *Quaternary Science Reviews* **148**: 176–191.